Emergence of Jets from Turbulence in the Shallow-Water Equations on an Equatorial Beta Plane

BRIAN F. FARRELL

Department of Earth and Planetary Sciences, Harvard University, Cambridge, Massachusetts

PETROS J. IOANNOU

Department of Physics, National and Capodistrian University of Athens, Athens, Greece

(Manuscript received 2 September 2008, in final form 24 April 2009)

ABSTRACT

Coherent jets, such as the Jovian banded winds, are a prominent feature of rotating turbulence. Shallow-water turbulence models capture the essential mechanism of jet formation, which is systematic eddy momentum flux directed up the mean velocity gradient. Understanding how this systematic eddy flux convergence is maintained and how the mean zonal flow and the eddy field mutually adjust to produce the observed jet structure constitutes a fundamental theoretical problem. In this work a shallow-water equatorial beta-plane model implementation of stochastic structural stability theory (SSST) is used to study the mechanism of zonal jet formation. In SSST a stochastic model for the ensemble-mean turbulent eddy fluxes is coupled with an equation for the mean jet dynamics to produce a nonlinear model of the mutual adjustment between the field of turbulent eddies and the zonal jets. In weak turbulence, and for parameters appropriate to Jupiter, both prograde and retrograde equatorial jets are found to be stable solutions of the SSST system, but only the prograde equatorial jet remains stable in strong turbulence. In addition to the equatorial jet, multiple midlatitude zonal jets are also maintained in these stable SSST equilibria. These midlatitude jets have structure and spacing in agreement with observed zonal jets and exhibit the observed robust reversals in sign of both absolute and potential vorticity gradient.

1. Introduction

Coherent jets are often observed in turbulent flows, with the banded winds of Jupiter constituting a familiar and frequently studied example (Ingersoll 1990; Vasavada and Showman 2005; Sánchez-Lavega et al. 2008). This phenomenon of spontaneous jet formation in turbulence has been studied observationally and theoretically (Rhines 1975; Williams 1979, 2003; Panetta 1993; Nozawa and Yoden 1997; Huang and Robinson 1998; Manfroi and Young 1999; Vallis and Maltrud 1993; Cho and Polvani 1996; Galperin et al. 2004; Lee 2005; Kaspi and Flierl 2007; Sokolov and Rintoul 2007), as well as in laboratory experiments (Krishnamurti and Howard 1981; Read et al. 2004, 2007). The primary mechanism maintaining planetary turbulent jets has been identified as eddy momentum flux systematically directed up the mean velocity gradient (Panetta 1993; Nozawa and Yoden 1997; Huang and Robinson 1998; Ingersoll et al. 2004; Salyk et al. 2006). This upgradient momentum flux is produced by shear straining of the eddy field by the mean flow, implying that the large-scale jets are maintained by a spectrally nonlocal interaction between the small-scale eddy field and the large-scale jets (Panetta 1993; Nozawa and Yoden 1997; Huang and Robinson 1998; Ingersoll et al. 2004; Salyk et al. 2006; Kitamura and Ishioka 2007).

Characteristics of the jets of Jupiter include prograde equatorial velocity, multiple midlatitude jets, asymmetry between prograde and retrograde jets such that the prograde jet is typically stronger and sharper than the retrograde jets, and substantial change in sign of the absolute vorticity gradient in the midlatitude retrograde jets (Limaye 1986; Porco et al. 2003; Read et al. 2006).

The central component of a theory for turbulent jet dynamics, that is, the method for obtaining the structure of the turbulence and the associated fluxes given the jet,

Corresponding author address: Brian Farrell, Department of Earth and Planetary Sciences, Harvard University, Geological Museum 452, 24 Oxford Street, Cambridge, MA 02138.
E-mail: farrell@seas.harvard.edu

DOI: 10.1175/2009JAS2941.1

is provided by a stochastic turbulence model (STM) (Farrell and Ioannou 1993a, 1994, 1995, 1996; DelSole and Farrell 1995; DelSole 1996; DelSole and Farrell 1996; Newman et al. 1997; Whitaker and Sardeshmukh 1998; Zhang and Held 1999; DelSole 2004). Once these fluxes are known, the equilibrium jet dynamical balance between the ensemble-mean turbulent momentum flux convergence and dissipation can be determined. This is the method of Stochastic Structural Stability Theory (SSST; Farrell and Ioannou 2003, 2008). The interaction between the large-scale jet structure and the field of eddy turbulence is nonlinear and results in a nonlinear trajectory for the jet and the ensemble-mean eddy field associated with it, which for parameter values in the shallow-water equations (SWEs) on an equatorial beta plane typical of Jovian conditions asymptotically approaches a stable equilibrium with multiple jets. This equilibrium arises from a linear instability of the coupled turbulence–mean flow system. This jet-forming instability is emergent from the interaction between the mean flow and the turbulence. The finite-amplitude equilibria can, for sufficiently low turbulence intensity, be connected continuously to the associated linear instabilities.

In this work, the convective excitation of turbulence observed in Jupiter's atmosphere (Gierasch et al. 2000; Ingersoll et al. 2000) is approximated as stochastic in both space and time and its amplitude taken as an independent parameter in the solution of the SSST system. Using this model we investigate both the formation and equilibration of jets in SWE equatorial beta-plane turbulence.

We find that if the turbulence is not too strong, and if a randomly structured small-amplitude initial zonal jet is prescribed, the equatorial jet equilibrium can be either prograde or retrograde, depending on the initial perturbation zonal velocity. This result is consistent with the existence of linear instability of the zonal jet free turbulent state to zonal jet perturbations that occurs in the presence of sufficient turbulence intensity. However, for parameter values used in our model simulations, as the turbulence level increases or the dissipation of the jet decreases, the nonlinear equilibrium equatorial jet speed increases and the retrograde equatorial jet ultimately loses structural stability. At this point the retrograde jet undergoes a catastrophic readjustment, from which it emerges as a prograde jet. On the other hand, the prograde equatorial jet persists as a stable equilibrium at higher turbulence intensity and/or lower jet dissipation, with correspondingly higher associated jet speed. The stability of both prograde and retrograde jets over a considerable parameter range is consistent with the mix of prograde and retrograde jets on the gaseous planets and in simulations of decaying turbulence initialized randomly (Kitamura and Ishioka 2007), as well as in simulations of forced turbulence (Huang and Robinson 1998; Scott and Polvani 2007, 2008). The phenomenon of retrograde jet destabilization occurs over a range of parameter values typical of Jupiter jet simulations but has not been verified to occur for all parameter values appropriate for the gaseous planets, particularly for Froude numbers of $O(1)$ or larger.

At low turbulence intensity, multiple nearly symmetric prograde and retrograde jets with low jet speed form in the midlatitudes. As turbulence intensity increases, the jet speed also increases, with the prograde jets becoming increasingly narrow while the retrograde jets assume a more rounded profile. These adjustments occur because as turbulence intensity rises, the retrograde jet encroaches on eddy stability boundaries, which results in modification of the jet structure by eddy momentum fluxes because these eddy fluxes diverge at the stability boundary (Farrell and Ioannou 2003). The stable equilibrium jets exhibit a substantial reversal in sign of both absolute and potential vorticity gradients. Such meridionally localized reversals of absolute vorticity gradient are a prominent feature of both observed and simulated jets (Limaye 1986; Read et al. 2006; Scott and Polvani 2007). Potential vorticity gradients, reversals of which are associated with necessary conditions for instability in the inviscid SWE system, change sign in approximate coincidence with absolute vorticity gradients in our jets, in observations, and in simulations (Read et al. 2006; Scott and Polvani 2007). We find that our jets remain stable with a limited extent of reversal of potential vorticity gradient, which implies, given the approximate coincidence of absolute and potential vorticity gradients, that jet spacing is close to the notional Rhines radius based on the mean velocity.[1] However, this meridional jet scale arises in SSST from a mechanism unrelated to the Rhines radius interpreted as a halting scale for two-dimensional turbulent cascades.

2. Dynamics of zonal jets in turbulence

A theory of zonal jet dynamics in turbulence was developed in Farrell and Ioannou (2003). This theory was applied to the problem of the formation of jets in barotropic turbulence in Farrell and Ioannou (2007) and to the problem of formation of jets in baroclinic turbulence in Farrell and Ioannou (2008). We now briefly review this theory in the context of the SWE.

[1] This follows from the vanishing of $\overline{q}_y = \beta - \overline{u}_{yy}$, implying $\beta \approx U/L^2$, where L is the meridional length scale and U is the velocity scale.

Consider the dynamics of a zonally unbounded shallow fluid layer confined by rigid walls to a meridional channel on an equatorial plane with a free upper boundary. The nondimensional equations for the zonal (x) velocity, u, meridional (y) velocity, v, and height, h, are

$$\partial_t u + u\partial_x u + v\partial_y u - f(y)v + \frac{1}{F^2}\partial_x h = -r_u - r(y)u + \nu\nabla^2 u, \quad (1a)$$

$$\partial_t v + u\partial_x v + v\partial_y v + f(y)u + \frac{1}{F^2}\partial_y h = -r_u - r(y)v + \nu\nabla^2 v, \quad (1b)$$

$$\partial_t h + u\partial_x h + v\partial_y h + (\partial_x u + \partial_y v)h = -r_h(h-1) - r(y)(h-1) + \nu\nabla^2 h. \quad (1c)$$

The Coriolis parameter for the equatorial beta plane is $f(y) = \beta y$ with $\beta = 2\omega/a$, where ω is the rotation rate of the planet and a is its radius. We will also consider the geophysical beta variation $f(y) = (\beta L_y/\pi)\sin(\pi y/L_y)$ over the channel interval $[-L_y/2, L_y/2]$. Rayleigh friction at rate r_u is included in the momentum equations and Newtonian cooling, at the rate r_h, in the height equation. We also include a latitudinally varying Rayleigh friction $r(y)$:

$$r(y) = r_s\left[1 - \tanh\left(\frac{y + L_y/2 - 1/2}{\delta_s}\right)\right] + r_s\left[1 + \tanh\left(\frac{y - L_y/2 + 1/2}{\delta_s}\right)\right] \quad (2)$$

that damps all fields, creating an absorbing sponge layer in the vicinity of the channel walls. Diffusive dissipation with coefficient ν is added to improve numerical stability.

Height is nondimensionalized by the equivalent depth of the fluid, H; the horizontal scales by a typical length scale, L; time by the period of rotation of the planet, $T = 2\pi/\omega$; and velocity by $U_0 = L/T$. The Froude number is $F = U_0/\sqrt{gH}$, with g being the gravitational acceleration. For Jupiter $T = 3.6 \times 10^4$ s, and with $L = 10^7$ m, the velocity scale is $U_0 = 278$ m s^{-1} and the nondimensional equatorial beta parameter is $\beta = 1.8$. In most of the examples $F = 0.3$, $r_s = 2$, $\delta_s = 0.5$, and $\nu = (6\delta y)^2$, where δy is the discretization interval in the meridional direction.

For the Jovian case we assume the fluid is forced by convection and is in a turbulent state. To model forcing of the mean jets by this turbulence, we use a stochastic turbulence model to obtain the ensemble mean eddy fluxes. The stochastic forcing and the damping parameters for Jupiter are not well known individually. What is known is the turbulent large-scale rms velocity, which is $O(5$ m s$^{-1})$, and the mean jet velocity, which is $O(100$ m s$^{-1})$ (Salyk et al. 2006). By adjusting the forcing and eddy damping to produce the observed level of turbulence, one can infer the linear mean jet dissipation rate required to produce the observed jet velocity. Combining the Lyapunov equation of the STM with the equation for the zonal mean flow, we obtain the autonomous deterministic equation set from which the jets in equilibrium with the turbulence can be determined (Farrell and Ioannou 2003). The development of these equations is now described in more detail.

Decompose the fields into zonal mean and fluctuations about the mean:

$$u = \overline{u} + u', \quad v = \overline{v} + v', \quad h = 1 + \overline{h} + h', \quad (3)$$

in which the bar denotes a zonal average, and assume weak meridional circulation. Neglecting[2] $\overline{v}$ and the eddy mass flux terms $\overline{v'h'}$, the zonal average of (1a) is

$$\partial_t \overline{u} = -\overline{v'Du'} - r_m\overline{u} - r(y)\overline{u} + \nu D^2\overline{u}, \quad (4)$$

where D denotes differentiation with respect to y and $1/r_m$ is the damping time of zonally averaged fields, which will be taken to be on the order of the radiative time scale $1/r_m \approx 1000$ Jovian days. The mean height $\overline{h}$ is obtained diagnostically by assuming geostrophic balance:

$$D\overline{h} = -F^2 f(y)\overline{u}. \quad (5)$$

The stochastic perturbation equations obtained from (1a)–(1c) are

$$\partial_t u' + \overline{u}\partial_x u' + [D\overline{u} - f(y)]v' + \frac{1}{F^2}\partial_x h' = -[r_u + r(y)]u' + \nu\nabla^2 u' + F_u\eta_u(t), \quad (6a)$$

$$\partial_t v' + \overline{u}\partial_x v' + f(y)u' + \frac{1}{F^2}\partial_y h' = -[r_u + r(y)]v' + \nu\nabla^2 v' + F_v\eta_v(t), \quad (6b)$$

$$\partial_t h' + \overline{u}\partial_x h' + D\overline{h}\,v' + (1 + \overline{h})(\partial_x u' + \partial_y v') = -[r_h + r(y)]h' + \nu\nabla^2 h' + F_h\eta_h(t). \quad (6c)$$

In the above equations the stochastic forcing terms $F_u\eta_u(t)$, $F_v\eta_v(t)$, and $F_h\eta_h(t)$ parameterize the structure and time variation of the convective excitation and the excitation from the nonlinear eddy–eddy scattering (cf. Farrell and Ioannou 2003). Because of zonal homogeneity, the fields can be expanded in a Fourier series with zonal

[2] We have verified that the Coriolis force associated with $\overline{v}$ is at least an order of magnitude smaller than the Reynolds stress term in (4).

wavenumber $\kappa = 2\pi m/L_x$, where L_x is the equatorial circumference and m is the global zonal wavenumber. The perturbation field at each wavenumber evolves according to

$$\frac{d\boldsymbol{\psi}}{dt} = \mathbf{A}_\kappa(\overline{u})\boldsymbol{\psi} + \sqrt{\epsilon}\mathbf{F}\boldsymbol{\eta}(t), \tag{7}$$

in which the state, $\boldsymbol{\psi}$, has been discretized on an equally spaced grid to form the state column vector: $[u_1, \ldots, u_n, v_1, \ldots, v_n, h_1, \ldots, h_n]^{\mathrm{T}}$, with subscript i denoting the value of the field at the ith discretization point and n the number of points. The associated dynamical operator $\mathbf{A}_\kappa(\overline{u})$ is expressed as a matrix using second-order finite differences. The parameter ϵ controls the excitation amplitude.

The eddy-induced acceleration $-\overline{v'Du'}$ is obtained under the ergodic assumption that the zonal mean is equal to the ensemble mean over realizations; that is,

$$\overline{v'Du'} = \langle v'Du' \rangle. \tag{8}$$

This ergodic assumption is accurate for the giant planets in which a large number of uncorrelated eddies force the mean flow. With this ergodic assumption, the eddy-induced acceleration $-\overline{v'Du'}$ can be obtained from the ensemble perturbation covariance as will be shown in (17) below.

Stochastic excitation of the SWE that is delta correlated in space and time excites space scales small compared with the Rossby radius and time scales small compared to f, so large divergent velocity fields are excited and a computationally expensive geostrophic adjustment needs to be resolved. To avoid this, the excitation is assumed to occur on space and time scales that excite nearly balanced velocity and height fields. We choose each column of the n_f columns of the $n \times n_f$ excitation matrix, $\mathbf{F}$, to excite the rotational component of the velocity by exciting the streamfunction proportional to $\exp[-(y - y_i)^2/\delta_f^2]$, where y_i is the y coordinate at the ith collocation point and $\delta_f = 1$, resulting in spatial correlation of the excitation over $L = 10^6$ m (this excitation matrix is assumed to be the same for all zonal wavenumbers, and we find it produces an approximately flat perturbation energy spectrum over the dynamically important zonal wavenumbers $m = 5$–60). A red noise process is used to correlate the above excitation structures in time. This red noise process is implemented by choosing the n_f red noise process $\boldsymbol{\eta}(t)$ to solve the equation

$$\frac{d\boldsymbol{\eta}}{dt} = -\frac{1}{\tau}\boldsymbol{\eta} + \sqrt{\frac{2}{\tau}}\mathbf{w}(t), \tag{9}$$

where τ is the autocorrelation time scale of the red noise process and $\mathbf{w}$ is a white noise process with zero mean and unit variance:

$$\langle \mathbf{w}(t) \rangle = 0, \quad \langle \mathbf{w}(t)\mathbf{w}^\dagger(s) \rangle = \mathbf{I}\boldsymbol{\delta}(t - s), \tag{10}$$

in which $\mathbf{I}$ is the identity matrix, $\langle \cdot \rangle$ denotes an ensemble average, and $\dagger$ denotes the Hermitian response. The factor $\sqrt{2/\tau}$ in (9) ensures that the red noise processes have unit variance. The covariance equation is obtained by combining (7) and (9) in the form

$$\frac{d}{dt}\begin{pmatrix} \boldsymbol{\psi}^\kappa \\ \boldsymbol{\eta}^\kappa \end{pmatrix} = \begin{pmatrix} \mathbf{A}^\kappa & \sqrt{\epsilon}\mathbf{F} \\ 0 & -\dfrac{1}{\tau}\mathbf{I} \end{pmatrix}\begin{pmatrix} \boldsymbol{\psi}^\kappa \\ \boldsymbol{\eta}^\kappa \end{pmatrix} + \begin{pmatrix} 0 \\ \sqrt{\dfrac{2}{\tau}}\mathbf{w} \end{pmatrix}. \tag{11}$$

The ensemble-mean covariance

$$\mathbf{C}^\kappa \equiv \begin{pmatrix} \mathbf{C}^\kappa_{\psi\psi} & \mathbf{C}^\kappa_{\psi\eta} \\ \mathbf{C}^\kappa_{\eta\psi} & \mathbf{C}^\kappa_{\eta\eta} \end{pmatrix} \equiv \begin{pmatrix} \langle \boldsymbol{\psi}^\kappa \boldsymbol{\psi}^{\kappa\dagger} \rangle & \langle \boldsymbol{\psi}^\kappa \boldsymbol{\eta}^{\kappa\dagger} \rangle \\ \langle \boldsymbol{\eta}^\kappa \boldsymbol{\psi}^{\kappa\dagger} \rangle & \langle \boldsymbol{\eta}^\kappa \boldsymbol{\eta}^{\kappa\dagger} \rangle \end{pmatrix} \tag{12}$$

of perturbations with zonal wavenumber, κ, evolves according to the time-dependent Lyapunov equation (Farrell and Ioannou 1996)

$$\frac{d\mathbf{C}^\kappa}{dt} = \hat{\mathbf{A}}^\kappa \mathbf{C}^\kappa + \mathbf{C}^\kappa \hat{\mathbf{A}}^{\kappa\dagger} + \hat{\mathbf{Q}}, \tag{13}$$

in which

$$\hat{\mathbf{A}}^\kappa = \begin{pmatrix} \mathbf{A}^\kappa & \sqrt{\epsilon}\mathbf{F} \\ 0 & -\dfrac{1}{\tau}\mathbf{I} \end{pmatrix} \tag{14}$$

is the operator of the perturbation dynamics augmented by the red noise process. The associated excitation is

$$\hat{\mathbf{Q}} = \begin{pmatrix} 0 & 0 \\ 0 & \dfrac{2}{\tau}\mathbf{I} \end{pmatrix}. \tag{15}$$

The acceleration induced by the entire field of eddies is the sum of the individual accelerations induced by each zonal wavenumber, κ:

$$-\overline{v'Du'} = -\sum_\kappa \overline{v'^\kappa Du'^\kappa}. \tag{16}$$

The contribution to this sum from each zonal wavenumber is obtained from the corresponding covariance, $\mathbf{C}^\kappa_{\psi\psi}$, in the following manner: If $\mathbf{P}_u$ is the operator that projects the state, $\boldsymbol{\psi}$, on the complex Fourier amplitude of its zonal velocity, u, and $\mathbf{P}_v$ is the corresponding projector on the amplitude of the meridional velocity, v, we then have

$$\sum_\kappa \overline{v'^\kappa Du'^\kappa} = \sum_\kappa \frac{1}{2}\Re(v'^\kappa Du'^{\kappa *}) = \sum_\kappa \frac{1}{2}\Re\Big[\mathrm{diag}\Big(\mathbf{P}_v \mathbf{C}^\kappa_{\psi\psi}\mathbf{P}_u^\dagger \mathbf{D}^\dagger\Big)\Big], \tag{17}$$

where $\Re$ denotes the real part, * denotes complex conjugation, and diag is the operation that forms a diagonal matrix with the elements of the column vector on which it operates or forms a vector from the diagonal of the matrix on which it operates.

The covariance evolution Eqs. (13) and the mean flow equation

$$\partial_t \overline{\mathbf{u}} = -\sum_\kappa \frac{1}{2}\Re\Big[\mathrm{diag}\Big(\mathbf{P}_v \mathbf{C}^\kappa_{\psi\psi}\mathbf{P}_u^\dagger \mathbf{D}^\dagger\Big)\Big] + \{-r\mathbf{I} + \mathrm{diag}[\mathbf{r}(y)] + \nu\mathbf{D}^2\}\delta\overline{u}, \tag{18}$$

form a deterministic set of equations for the mean wind, $\overline{\mathbf{u}}$, and the eddy covariances, $\mathbf{C}^\kappa_{\psi\psi}$, that governs their time-dependent coevolution. These are the SSST equations with which we can determine both the equilibrium jets and their structural stability. The equation for the mean (18) is linear in both $\mathbf{C}^\kappa$ and $\overline{\boldsymbol{u}}$. The nonlinearity in the SSST equations appears only in the covariance equation (13) which contains products of components of $\overline{\boldsymbol{u}}$ (as $\mathbf{A}^\kappa$ depends linearly on $\overline{\boldsymbol{u}}$) and components of $\mathbf{C}^\kappa$. This nonlinear system is globally stable and its typical temporal asymptotic solutions are steady jets; although limit cycle and chaotic trajectories are supported for some parameter values (Farrell and Ioannou 2003).

3. Mechanism of jet formation

At sufficiently low turbulence levels, controlled by the variance of the stochastic excitation ϵ, eddy–mean flow interaction is inadequate to overcome dissipation, jet growth does not occur, and the mean flow remains constant and close to zero. We call this nearly motionless state the zero state. The stability of the zero state can be studied by perturbing the SSST system [(13) and (18)] and investigating the eigenvalues of the corresponding coupled perturbation equations for $\delta\mathbf{C}$, the perturbation covariance, and $\delta\overline{\boldsymbol{u}}$, the perturbation mean zonal flow:

$$\partial_t \delta\overline{\mathbf{u}} = -\sum_\kappa \frac{1}{2}\Re\Big[\mathrm{diag}\Big(\mathbf{P}_v \delta\mathbf{C}^\kappa_{\psi\psi}\mathbf{P}_u^\dagger \mathbf{D}^\dagger\Big)\Big] - \{r_m\mathbf{I} + \mathrm{diag}[\mathbf{r}(y)] - \nu\boldsymbol{D}^2\}\delta\overline{\boldsymbol{u}}, \tag{19}$$

$$\partial_t \delta\mathbf{C}^\kappa = \hat{\mathbf{A}}_0^\kappa \delta\mathbf{C}^\kappa + \delta\mathbf{C}^\kappa \hat{\mathbf{A}}_0^{\kappa\dagger} + \epsilon\Big(\delta\hat{\mathbf{A}}^\kappa \mathbf{C}_0^\kappa + \mathbf{C}_0^\kappa \delta\hat{\mathbf{A}}^{\kappa\dagger}\Big). \tag{20}$$

In Eq. (20) $\mathbf{C}_0^\kappa$ is the eddy covariance maintained at equilibrium by unit excitation $\epsilon = 1$ when the background flow is the zero state with associated linear operator $\hat{\mathbf{A}}_0^\kappa$. Equation (20) depends linearly on $\delta\mathbf{C}^\kappa$, linearly on $\delta\overline{\boldsymbol{u}}$ (because the perturbation linear operator $\delta\hat{\mathbf{A}}^\kappa$ is a linear function of $\delta\overline{\boldsymbol{u}}$), and linearly on ϵ (because the covariance at equilibrium is a linear function of the excitation level). For a critical value of the excitation ϵ_c, the SSST perturbation system becomes unstable, and for values larger than the critical a new mean flow arises, which for excitations close to ϵ_c has nearly the same structure as the most unstable eigenfunction of the SSST perturbation equations.

The critical ϵ_c and the structure of the eigenfunctions (denoted with the subscript *eig*)

$$\begin{pmatrix} \delta\overline{\boldsymbol{u}}_{\mathrm{eig}} \\ \delta\mathbf{C}^\kappa_{\mathrm{eig}} \end{pmatrix} \tag{21}$$

at the bifurcating point can be obtained with economy when at the bifurcating point the top eigenvalue of (19) and (20) is real and zero (i.e., when the principle of exchange of stability holds). When this is true, the structure of the instability at the bifurcating point can be studied very simply because at ϵ_c Eq. (20) implies that the eigenfunction $\delta\mathbf{C}^\kappa_{\mathrm{eig}}$ corresponding to the zero eigenvalue must satisfy

$$\hat{\mathbf{A}}_0^\kappa \delta\mathbf{C}^\kappa_{\mathrm{eig}} + \delta\mathbf{C}^\kappa_{\mathrm{eig}}\hat{\mathbf{A}}_0^{\kappa\dagger} = -\epsilon_c\Big(\delta\hat{\mathbf{A}}^\kappa \mathbf{C}_0^\kappa + \mathbf{C}_0^\kappa \delta\hat{\mathbf{A}}^{\kappa\dagger}\Big). \tag{22}$$

This Lyapunov equation makes clear that $\delta\mathbf{C}^\kappa_{\mathrm{eig}}$ becomes a linear function of $\delta\overline{\boldsymbol{u}}_{\mathrm{eig}}$ and ϵ_c and the perturbation eddy-induced acceleration in (19) can be written as

$$-\sum_\kappa \frac{1}{2}\Re\Big[\mathrm{diag}\Big(\mathbf{P}_v \delta\mathbf{C}^\kappa_{\psi\psi\mathrm{eig}}\mathbf{P}_u^\dagger \mathbf{D}^\dagger\Big)\Big] = \epsilon_c \mathbf{M}\delta\overline{\boldsymbol{u}}_{\mathrm{eig}}, \tag{23}$$

where $\mathbf{M}$ is a linear operator. Substituting (23) in (19), we obtain in the absence of sponge layers and diffusive damping that $\delta\overline{\boldsymbol{u}}_{\mathrm{eig}}$ is an eigenfunction of $\mathbf{M}$:

$$\epsilon_c \mathbf{M}\delta\overline{\boldsymbol{u}}_{\mathrm{eig}} = r_m \delta\overline{\boldsymbol{u}}_{\mathrm{eig}}. \tag{24}$$

The critical destabilizing ϵ_c for an eigenfunction is given by $\epsilon_c = r_m/\lambda$, where $\lambda > 0$ is a corresponding positive eigenvalue of $\mathbf{M}$.

The operator $\mathbf{M}$ in (24) can be written using (17) as

$$M_{ij} = -\frac{\partial\langle(v'Du')\rangle_i}{\partial\overline{u}_j}, \tag{25}$$

in which $\mathbf{M}$ can be interpreted as determining the sensitivity of the zonal mean eddy momentum flux convergence for unit turbulence excitation ($\epsilon_c = 1$) to small changes in the zonal mean wind; specifically, we interpret $-\langle(v'Du')\rangle_i$ to be, for unit excitation, the eddy acceleration induced at the ith collocation point by a zonal mean wind perturbation at the jth collocation point, $\overline{u}_j$.

For simplicity assume an eddy field restricted to have a single perturbation zonal wavenumber, m, and obtain the critical ϵ_c and the corresponding top eigenfunction of $\epsilon_c\mathbf{M} - r_m\mathbf{I}$ as a function of m. The eigenfunction of $\epsilon_c\mathbf{M} - r_m\mathbf{I}$ with zero growth gives the mean flow structure that will emerge at small but supercritical $\epsilon > \epsilon_c$. At the associated ϵ_c the zero state becomes structurally unstable and jets emerge from this monochromatic eddy field. The critical rms turbulence intensity r_m/λ_m, where λ_m is the top positive eigenvalue of $\mathbf{M}$, is shown as a function of zonal wavenumber m in Fig. 1. The critical excitation ϵ_c decreases rapidly with eddy perturbation zonal wavenumber m, implying that if the high eddy perturbation zonal wavenumbers are not suppressed, the flow will be organized (at least for sufficiently small zonal wind perturbations) by these high-zonal-wavenumber eddies. Such an increase in forcing of the mean jet with increase in zonal perturbation wavenumber was noted by Kitamura and Ishioka (2007).

The top eigenfunctions of $\epsilon_c\mathbf{M} - r_m\mathbf{I}$ for eddy zonal wavenumbers $m = 20$, 40, 60 are shown in Fig. 2. The underlying mechanism of jet formation producing these eigenfunctions can be traced to the general property that shearing of turbulence produces an upgradient momentum flux that is equivalent to an antidiffusion (Starr 1968; Farrell and Ioannou 1993b, 2007).

We can further probe the organization of turbulent eddy momentum fluxes by zonal jets by imposing an infinitesimal velocity perturbation centered at the equator of the form $\delta\overline{u} = \exp[-(y/\Delta y)^2]$. With $\Delta y = 1$, the resulting eddy-turbulence-induced fractional time rate of change of the mean flow for excitation by representative zonal wavenumbers is shown in Fig. 3. Unlike the eigenfunctions shown in Fig. 2, these test functions induce momentum flux convergence that will not preserve their form. Both Figs. 2 and 3 show linear perturbation results implying that either sign of jet perturbation is equally likely to be destabilized with an e-folding time on the order of 300 Jovian days. It follows that either a prograde or a retrograde equatorial jet can emerge at small turbulence levels depending on initial conditions, a result consistent with the simulations of Kitamura and Ishioka (2007).

One implication of the antidiffusive upgradient momentum flux produced by perturbations to zonal velocity is that the eigenfunctions of $\mathbf{M}$ are approximately the eigenfunctions of the diffusion operator, which explains the nearly harmonic form of the initial mean zonal jets that grow out of the turbulence field (cf. Fig. 2).

Turbulent eddies are distributed over all perturbation zonal scales and the eigenfunctions of the total sensitivity matrix (23) formed as the sum over contributions from all perturbation zonal wavenumbers depend on this distribution. However, as we have seen, the higher zonal wavenumbers produce disproportionately greater flux, so they dominate the tendency unless their amplitude falls off very rapidly with wavenumber.

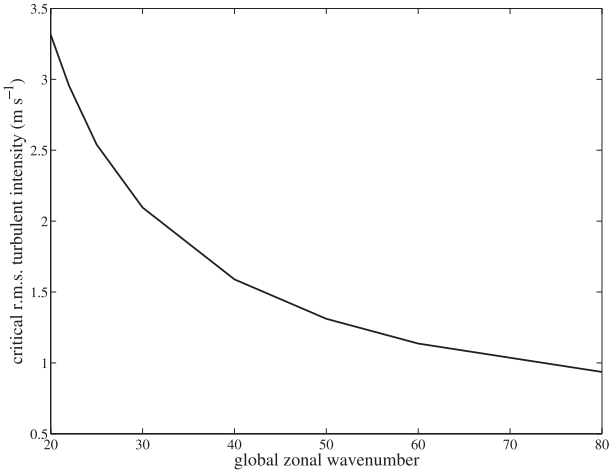

FIG. 1. Critical rms turbulence intensity, resulting from excitation $\epsilon = r_m/\lambda_m$, required to destabilize the top eigenfunction of the eddy–mean flow interaction operator $\mathbf{M}$ with eigenvalue $\lambda_m > 0$ as a function of global zonal wavenumber m. Parameters are $r_m = 10^{-3}$, $F = 0.3$, $r = 0.15$, $r_h = 0.15$, and $\nu = 0$.

4. Formation and equilibration of prograde and retrograde equatorial jets

We wish to study the formation and equilibration of the equatorial jet and choose as a bifurcation parameter the variance of the stochastic excitation maintaining the turbulence, ε. For very small values of this excitation the equilibrium flow is nearly zero.[3] As the excitation increases, a critical value is reached at which, with equal probability given random initial conditions, either a prograde or a retrograde jet emerges as an instability at a bifurcation point. This instability subsequently equilibrates at finite amplitude and the maximum of the equilibrium zonal jet wind speed at the equator for Jovian parameters as a function of rms velocity of the turbulence that would be maintained by the excitation if it were applied to the zero state is shown in Fig. 4. The turbulence level observed on Jupiter[4] (Salyk et al. 2006)

[3] The motionless state is not exactly an equilibrium because of spatial inhomogeneity of the Coriolis parameter and dissipation near the boundaries.

[4] This turbulence level is controlled by the stochastic forcing, parameterizing convection, and the eddy damping. These values are uncertain, but for determining the eddy fluxes the intensity of the turbulence resulting is the relevant variable, not the individual value of the excitation and damping.

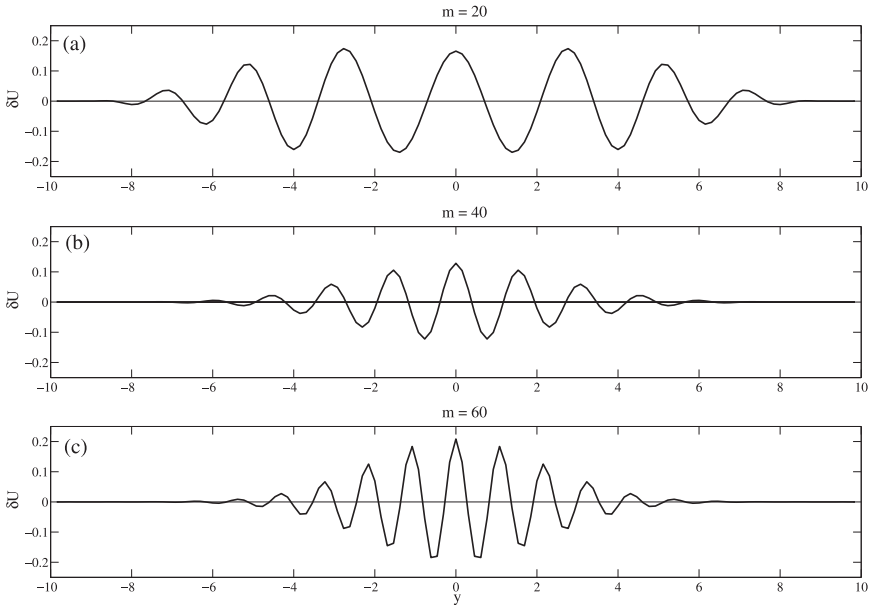

FIG. 2. Meridional structure of the most unstable eigenfunction of the eddy–mean flow sensitivity operator, **M**, for four global zonal wavenumbers, m: (a) $m = 20$, (b) $m = 40$, (c) $m = 60$. Parameters are $F = 0.3$, $r = 0.15$, $r_h = 0.15$, and $\nu = 0$. The critical rms turbulence intensity to destabilize these eigenfunctions is respectively 3.3, 1.6, and 1.1 m s^{-1}.

is also indicated in Fig. 4. The equilibrium prograde and retrograde jet structure at selected turbulence levels along the equilibrium curves in Fig. 4 are shown in Figs. 5 and 6, together with their associated absolute and potential vorticity gradients. The jet zonal wind maximum increases with increase in turbulence, and to remain stable the jet shape adjusts to lie near the Ripa (1983) necessary condition for instability primarily by broadening the retrograde jets. The Ripa necessary condition is an inviscid criterion that requires that potential vorticity gradient

$$Q_y = (1 + \overline{h})^{-1}[\beta(y) - D^2\overline{u} + F^2 f(y) Q\overline{u}] \qquad (26)$$

change sign for instability to arise (here $Q = [f(y) - D\overline{u}]/(1 + \overline{h})$. We find that jet structure at marginal stability avoids a large sign change in potential vorticity gradient such that at these parameter values, as the turbulence variance increases, the retrograde equatorial jet eventually is unable to maintain a stable equilibrium and catastrophically reconfigures into a prograde jet.

Zonal mean jets for Jovian parameters with a variable Coriolis parameter are shown together with their absolute and potential vorticity gradients in Fig. 7. The absolute and potential vorticity gradients are close, as they are also seen to be in observations (Read et al. 2006), and become negative predominantly where the jets are retrograde, again in agreement with observations. The potential vorticity exhibits a staircase structure as seen in Fig. 8, again in agreement with observations and simulations (Read et al. 2006; Scott and Polvani 2007). Note that negative potential vorticity gradients are not

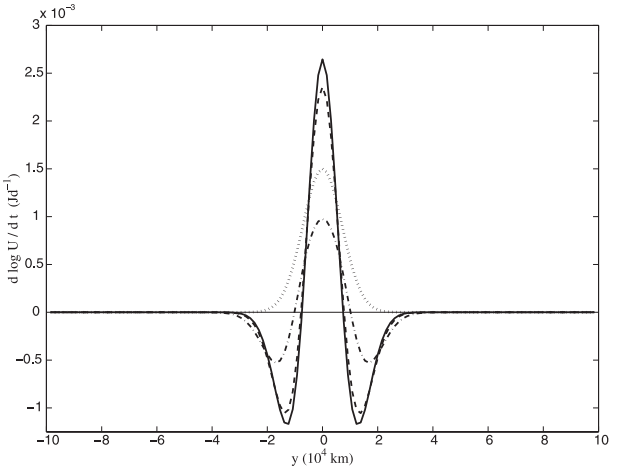

FIG. 3. Meridional structure of the mean flow acceleration $d\log(U)/dt$ (in inverse Jovian days) induced by eddy momentum flux convergence when the background zero state mean flow is infinitesimally perturbed in the form $\delta\overline{u} = \exp[-(y/\Delta y)^2]$ (dotted) for an eddy field with global zonal wavenumber $m = 20$ (dashed–dotted), $m = 40$ (dashed), and $m = 60$ (solid). The parameters are $\Delta y = 1$, $F = 0.3$, $r = 0.15$, $r_h = 0.15$, and $\nu = 0$; the rms turbulent intensity is 5 m s^{-1}.

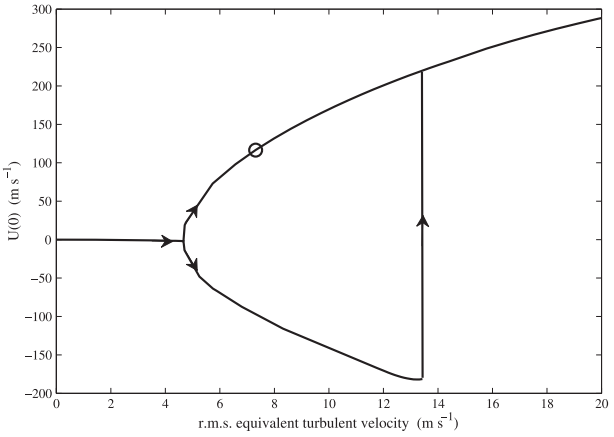

FIG. 4. Equilibrium equatorial jet speed as a function of turbulence intensity expressed as the rms velocity that would be maintained by the stochastic excitation of the state with no zonal mean flow. Both prograde and retrograde jets bifurcate from this zero state. The circle indicates approximate conditions for the equatorial jet of Jupiter. Arrows indicate continuation of the equilibrium states. A retrograde equatorial jet is not supported at rms turbulence intensity greater than 13.5 m s^{-1}. The case shown is for an equatorial β plane with Jovian planetary parameters $F = 0.3$, $\beta = 1.7952$, $r = 0.2$, $r_h = 0.2$, $\nu = 0.02$, $r_m = 10^{-3}$, and $\tau = 5$. A sponge layer starts one unit before the boundary and the sponge layer is not forced. The eddy field comprises global zonal wavenumbers $m = 5$, 10, 15, 20, 25, 28, 30, 32, and 34; the equatorial circumference is $L_x = 40$.

consistent with theories for jet formation based on diffusive mixing of planetary potential vorticity (Dritschel and McIntyre 2008). With these parameters the equatorial flow could equally have been retrograde, as shown

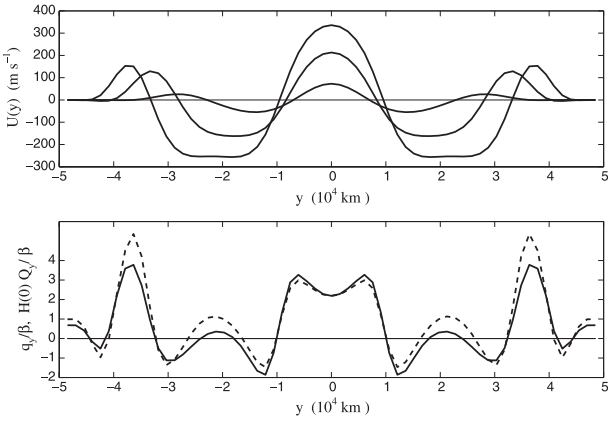

FIG. 5. (top) Meridional structure of the equilibrium prograde equatorial jets for turbulence intensities 5.75, 13, and 26 m s^{-1} from the example shown in Fig. 4. The stronger jets correspond to higher intensity. (bottom) Normalized potential vorticity gradient $H(0)Q_y/\beta$ (solid) and absolute vorticity gradient q_y/β (dashed) of the strongest jet in the top panel. Both vorticity gradients change sign, consistent with observations.

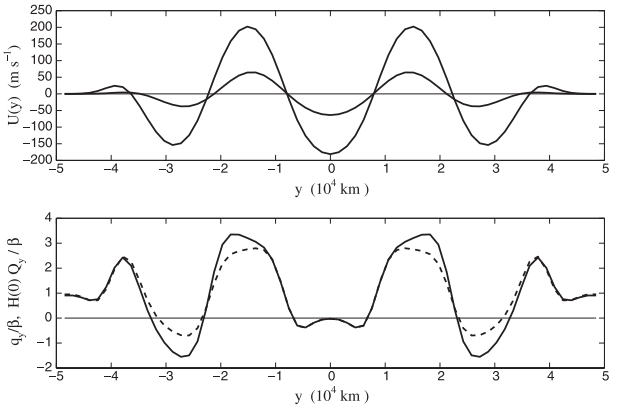

FIG. 6. (top) Meridional structure of the equilibrium retrograde equatorial jets for turbulence intensities 5.75 and 13 m s^{-1} from the example shown in Fig. 4. The stronger jet corresponds to the higher intensity. (bottom) Normalized potential vorticity gradient $H(0)Q_y/\beta$ (solid) and absolute vorticity gradient q_y/β (dashed) of the stronger jet in the top panel. Both vorticity gradients change sign, consistent with observations.

in the left panel of Fig. 9. But if the excitation is increased by 15% (or equivalently the dissipation of the jet decreased by a similar factor), the retrograde jet loses structural stability and a prograde equilibrium eventually emerges, as shown in the right panel of Fig. 9. This transition is shown in the center panel of Fig. 8. The prograde jet shown at the right subsequently converges to a stable fixed point with essentially the same

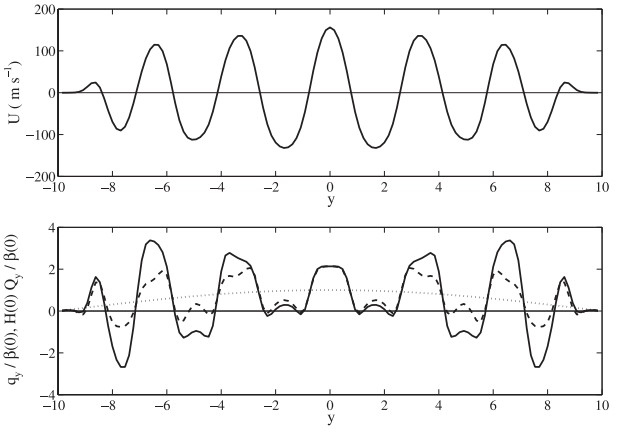

FIG. 7. (top) Meridional structure of the jets for Jovian conditions. The stochastic excitation is that which would maintain 8.2 m s^{-1} rms variance in the absence of any flow. (bottom) Meridional structure of normalized potential vorticity gradient $H(0)Q_y/\beta$ (solid) and absolute vorticity gradient q_y/β (dashed); the planetary vorticity gradient is also shown (dotted). The eddy parameters are $r = 0.15$, $r_h = 0.45$, and $\nu = 0$; the mean flow parameters are $\nu = 0.02$ and $r = 0.15$. The zonal wavenumbers included are $m = 5$, 8, 10, 14, 20, 30, 40, 50, 60.

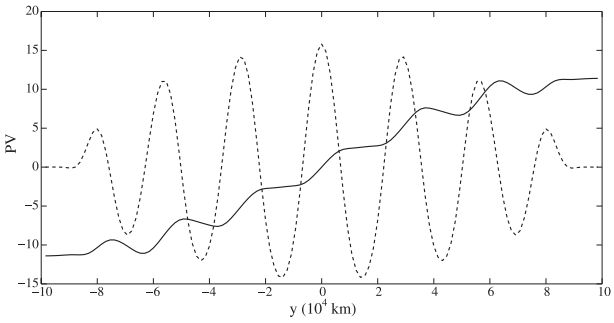

FIG. 8. Meridional structure of PV for the jet shown in Fig. 7 (solid). Also shown is the associated jet scaled to fit (dashed). The PV exhibits staircase structure.

structure. This example shows how SSST dynamics naturally explain the phenomenon of jet coalescence and, given that SSST is linear in the eddy dynamics, demonstrates that jet coalescence is not necessarily related to a turbulent cascade.

5. Conclusions

Zonal jets, such as are observed on Jupiter, emerge spontaneously from turbulence in the absence of jet scale forcing. The physical mechanism giving rise to and maintaining these jets is turbulent eddy fluxes systematically organized, through interaction with the jet, to support the jet structure. This phenomenon is associated with a ubiquitous instability of turbulent fluids to jet formation, which occurs because turbulent eddies are organized by an appropriately configured perturbation zonal jet to produce exactly the momentum fluxes required to amplify that jet. This jet formation mechanism essentially emerges from the interaction between the mean state and the turbulence. The problem of capturing this emergent instability analytically is solved by SSST. The SSST equations comprise a stochastic turbulence model to obtain the eddy fluxes coupled to an evolution equation for the mean flow.

In this work we applied SSST to jet formation in the turbulent SWE on an equatorial beta plane to model emergence and equilibration of the zonal jets of Jupiter. We find for parameter values appropriate for Jupiter that these jets form spontaneously as a linear instability when turbulence reaches sufficient intensity and grow until reaching a nonlinear equilibrium. Therefore, at low turbulence levels both prograde and retrograde equatorial jets form and we find that both subsequently progress to form stable equilibria, but for sufficiently high turbulence levels and for Froude numbers used in the examples in this work only the prograde equatorial jet can be maintained as an equilibrium state. In the midlatitudes multiple jets are maintained at equilibrium with amplitude decreasing poleward. As turbulence intensity increases, the equatorial jets become increasingly asymmetric with the retrograde jet widening. This jet structure evolution with increasing turbulence intensity is characteristic of a progression that contrives to maintain the eddy stability of the jet despite increasing jet

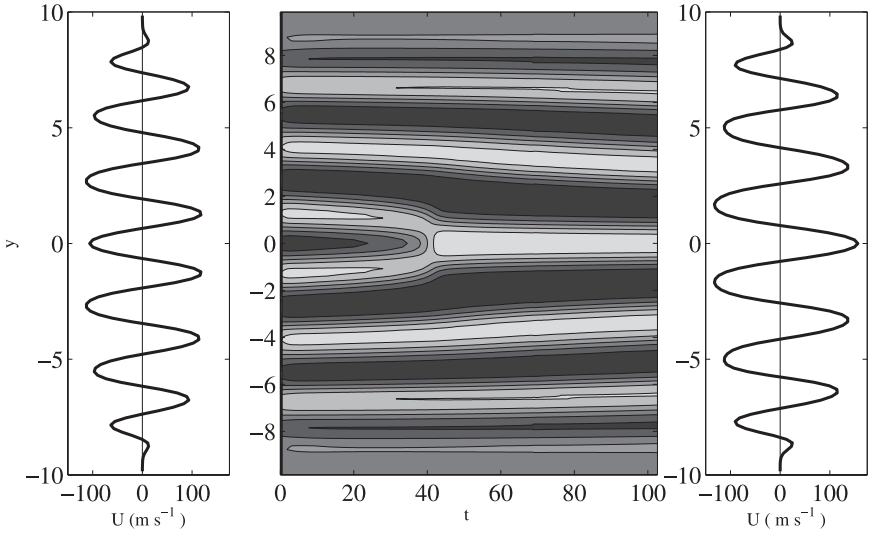

FIG. 9. (left) The initial condition consisting of an equilibrium retrograde jet for the parameters of Fig. 7 and equivalent turbulent intensity 8.2 m s^{-1}. At $t = 0$ the forcing is increased 15%, producing a turbulent intensity of 9.4 m s^{-1} and the retrograde jet is no longer an equilibrium. (right) The equatorial wind reverses at $t = 37.5$, giving rise at $t = 47$ to the equilibrium prograde jet. (center) Contours of zonal velocity as a function of latitude and time.

amplitude. In agreement with the observed Jovian jets (Read et al. 2006) and simulations (Scott and Polvani 2007), we find the retrograde midlatitude jets both satisfy the Ripa (1983) necessary condition for instability and exhibit pronounced change in sign of absolute vorticity gradients. We note that mixing of planetary potential vorticity cannot produce such reversals of potential vorticity gradient.

The mechanism of jet formation we have described is captured by SSST, which provides a new perspective on the interaction between turbulence and mean flows. As we have briefly discussed, the dynamics of this interaction can be understood more deeply by further analyzing the functional derivative of momentum flux divergence with mean jet velocity perturbations, a study that is in preparation.

Acknowledgments. This work was partially supported by NSF ATM-0736022.

REFERENCES

Cho, J. Y.-K., and L. M. Polvani, 1996: The morphogenesis of bands and zonal winds in the atmospheres on the giant outer planets. *Science,* **273,** 335–337.

DelSole, T., 1996: Can quasigeostrophic turbulence be modeled stochastically? *J. Atmos. Sci.,* **53,** 1617–1633.

——, 2004: Stochastic models of quasigeostrophic turbulence. *Surv. Geophys.,* **25,** 107–194.

——, and B. F. Farrell, 1995: A stochastically excited linear system as a model for quasigeostrophic turbulence: Analytic results for one- and two-layer fluids. *J. Atmos. Sci.,* **52,** 2531–2547.

——, and ——, 1996: The quasi-linear equilibration of a thermally maintained, stochastically excited jet in a quasigeostrophic model. *J. Atmos. Sci.,* **53,** 1781–1797.

Dritschel, D. G., and M. E. McIntyre, 2008: Multiple jets as PV staircases: The Phillips effect and the resilience of eddy-transport barriers. *J. Atmos. Sci.,* **65,** 855–874.

Farrell, B. F., and P. J. Ioannou, 1993a: Stochastic dynamics of baroclinic waves. *J. Atmos. Sci.,* **50,** 4044–4057.

——, and ——, 1993b: Stochastic forcing of perturbation variance in unbounded shear and deformation flows. *J. Atmos. Sci.,* **50,** 200–211.

——, and ——, 1994: A theory for the statistical equilibrium energy spectrum and heat flux produced by transient baroclinic waves. *J. Atmos. Sci.,* **51,** 2685–2698.

——, and ——, 1995: Stochastic dynamics of the midlatitude atmospheric jet. *J. Atmos. Sci.,* **52,** 1642–1656.

——, and ——, 1996: Generalized stability theory. Part I: Autonomous operators. *J. Atmos. Sci.,* **53,** 2025–2040.

——, and ——, 2003: Structural stability of turbulent jets. *J. Atmos. Sci.,* **60,** 2101–2118.

——, and ——, 2007: Structure and spacing of jets in barotropic turbulence. *J. Atmos. Sci.,* **64,** 3652–3665.

——, and ——, 2008: Formation of jets by baroclinic turbulence. *J. Atmos. Sci.,* **65,** 3353–3375.

Galperin, B., H. Nakano, H.-P. Huang, and S. Sukoriansky, 2004: The ubiquitous zonal jets in the atmospheres of giant planets and Earth's oceans. *Geophys. Res. Lett.,* **31,** L13303, doi:10.1029/2004GL019691.

Gierasch, P. J., and Coauthors, 2000: Observation of moist convection in Jupiter's atmosphere. *Nature,* **403,** 628–630.

Huang, H.-P., and W. A. Robinson, 1998: Two-dimensional turbulence and persistent zonal jets in a global barotropic model. *J. Atmos. Sci.,* **55,** 611–632.

Ingersoll, A. P., 1990: Atmospheric dynamics of the outer planets. *Science,* **248,** 308–315.

——, and Coauthors, 2000: Moist convection as an energy source for the large-scale motions in Jupiter's atmosphere. *Nature,* **403,** 630–632.

——, and Coauthors, 2004: Dynamics of Jupiter's atmosphere. *Jupiter: The Planet, Satellites, and Magnetosphere,* F. Bagenal, T. E. Dowling, and W. B. McKinnon, Eds., Cambridge University Press, 105–128.

Kaspi, Y., and G. R. Flierl, 2007: Formation of jets by baroclinic instability on gas planet atmospheres. *J. Atmos. Sci.,* **64,** 3177–3194.

Kitamura, Y., and K. Ishioka, 2007: Equatorial jets in decaying shallow-water turbulence on a rotating sphere. *J. Atmos. Sci.,* **64,** 3340–3353.

Krishnamurti, R., and L. N. Howard, 1981: Large-scale flow generation in turbulent convection. *Proc. Natl. Acad. Sci. USA,* **78,** 1981–1985.

Lee, S., 2005: Baroclinic multiple zonal jets on the sphere. *J. Atmos. Sci.,* **62,** 2484–2498.

Limaye, S. S., 1986: Jupiter: New estimates of the mean zonal flow at the cloud level. *Icarus,* **65,** 335–352.

Manfroi, A. J., and W. R. Young, 1999: Slow evolution of zonal jets on the beta plane. *J. Atmos. Sci.,* **56,** 784–800.

Newman, M., P. D. Sardeshmukh, and C. Penland, 1997: Stochastic forcing of the wintertime extratropical flow. *J. Atmos. Sci.,* **54,** 435–455.

Nozawa, T., and Y. Yoden, 1997: Formation of zonal band structure in forced two-dimensional turbulence on a rotating sphere. *Phys. Fluids,* **9,** 2081–2093.

Panetta, R. L., 1993: Zonal jets in wide baroclinically unstable regions: Persistence and scale selection. *J. Atmos. Sci.,* **50,** 2073–2106.

Porco, C. C., and Coauthors, 2003: *Cassini* imaging of Jupiter's atmosphere, satellites, and rings. *Science,* **299,** 1541–1547.

Read, P. L., Y. H. Yamazaki, S. R. Lewis, P. D. Williams, K. Miki-Yamazaki, J. Sommeria, H. Didelle, and A. Fincham, 2004: Jupiter's and Saturn's convectively driven banded jets in the laboratory. *Geophys. Res. Lett.,* **31,** L22701, doi:10.1029/2004GL020106.

——, P. J. Gierasch, B. J. Conrath, A. Simon-Miller, T. Fouchet, and Y. H. Yamazaki, 2006: Mapping potential-vorticity dynamics on Jupiter. I: Zonal-mean circulation from *Cassini* and *Voyager I* data. *Quart. J. Roy. Meteor. Soc.,* **132,** 1577–1603.

——, Y. H. Yamazaki, S. R. Lewis, P. D. Williams, R. Wordsworth, and K. Miki-Yamazaki, 2007: Dynamics of convectively driven banded jets in the laboratory. *J. Atmos. Sci.,* **64,** 4031–4052.

Rhines, P. B., 1975: Waves and turbulence on a beta plane. *J. Fluid Mech.,* **69,** 417–433.

Ripa, P., 1983: General stability conditions for zonal flows in a one-layer model on the β-plane or the sphere. *J. Fluid Mech.,* **126,** 463–489.

Salyk, C., A. P. Ingersoll, J. Lorre, A. Vasavada, and A. D. Del Genio, 2006: Interaction between eddies and mean flow in Jupiter's atmosphere: Analysis of *Cassini* imaging data. *Icarus,* **185,** 430–442.

Sánchez-Lavega, A., and Coauthors, 2008: Depth of a strong Jovian jet from a planetary-scale disturbance driven by storms. *Nature,* **451,** 437–440.

Scott, R. K., and L. M. Polvani, 2007: Forced-dissipative shallow-water turbulence on the sphere and the atmospheric circulation of the giant planets. *J. Atmos. Sci.,* **64,** 3158–3176.

——, and ——, 2008: Equatorial superrotation in shallow atmospheres. *Geophys. Res. Lett.,* **35,** L24202, doi:10.1029/2008GL036060.

Sokolov, S., and S. Rintoul, 2007: Multiple jets of the Antarctic Circumpolar Current south of Australia. *J. Phys. Oceanogr.,* **37,** 1394–1412.

Starr, V., 1968: *Physics of Negative Viscosity Phenomena*. McGraw-Hill, 256 pp.

Vallis, G. K., and M. E. Maltrud, 1993: Generation of mean flows and jets on a beta plane and over topography. *J. Phys. Oceanogr.,* **23,** 1346–1362.

Vasavada, A. R., and A. P. Showman, 2005: Jovian atmospheric dynamics: An update after *Galileo* and *Cassini*. *Rep. Prog. Phys.,* **68,** 1935–1996.

Whitaker, J. S., and P. D. Sardeshmukh, 1998: A linear theory of extratropical synoptic eddy statistics. *J. Atmos. Sci.,* **55,** 237–258.

Williams, G. P., 1979: Planetary circulations: 2. The Jovian quasi-geostrophic regime. *J. Atmos. Sci.,* **36,** 932–969.

——, 2003: Jet sets. *J. Meteor. Soc. Japan,* **81,** 439–476.

Zhang, Y., and I. M. Held, 1999: A linear stochastic model of a GCM's midlatitude storm tracks. *J. Atmos. Sci.,* **56,** 3416–3435.